JMEPEG (2009) 18:925–934
DOI: 10.1007/s11665-008-9320-7

1059-9495/$19.00

Thermal Expansion Coefficient and Mechanical Properties of Friction Stir Welded Invar (Fe-36%Ni)

Bharat K. Jasthi, William J. Arbegast, and Stanley M. Howard

(Submitted February 26, 2008; in revised form October 3, 2008)

Two high-temperature pin tools, one a polycrystalline cubic BN and the other of W-25%Re, were used to friction stir weld 12.7 mm thick Invar (Fe-36%Ni) plate. Successful welds were produced at a rotational speed of 600 rev min^{-1} and travel speeds of 76, 102, and 127 mm min^{-1}. The coefficient of thermal expansion, tensile strength, and microhardness of the welds were measured and found to be essentially unchanged from the parent material. The measured elongation was 52% for the parent material and 30 and 37% for welds made with the W-Re and the polycrystalline cubic BN pin tools. Both pin tools produced comparable welds but the W-Re tool exhibited more wear and left small wear remnants in the weld especially at the weld plunge.

Keywords coefficient of thermal expansion, friction stir welding, Invar, PCBN, W-25%Re

1. Introduction

The purpose of this investigation was to determine if friction stir welding (FSW) could produce a high-quality Invar weld that exhibits the same coefficient of thermal expansion as the parent material, thereby overcoming the problems observed in Invar fusion welding.

Invar is a Fe-36%Ni alloy with a face centered cubic structure. It has excellent toughness, good formability, and very low coefficient of thermal expansion (CTE) up to 400 °C. Traditionally, it has been used primarily in precision measuring devices and standards where dimensional stability over a wide temperature range is required. More recently Invar is being used for cryogenic liquid transfer systems and many defense, aerospace, and research applications that require complex, high-precision, and close-tolerance tooling. This tooling is used for composite structure fabrication. The CTE of Invar can be matched to that of the molding material and has the valued advantage of excellent durability.

Even though Invar has ideal properties for such applications, its use is greatly complicated by the difficulty in maintaining its properties when joined by fusion welding. Such welding results in solidification cracking, porosity, and reheating cracking when a matching CTE filler metal is used (Ref 1-4). These problems can be addressed with the addition of Ti, Mn, and increased C in the filler metal; however, these alloying additions lead to a CTE mismatch in the weld regions (Ref 3). Attempts to obviate these problems by using fillerless fusion welding are reported to have resulted in unpredictable ductility and are to be avoided for structures where reliability is needed (Ref 3).

FSW technology was invented in 1991 by The Welding Institute (TWI), UK (Ref 5). The underlying principle is the conversion to thermal energy the mechanical energy of a rotating, nonconsumable pin tool plunged into the abutted edges of the plates to be welded. During this process, heat is generated within the material from (1) friction between the pin tool and weld material and (2) severe plastic deformation of the material being welded. Temperature may approach, but is unlikely to reach, the melting point of the material (Ref 6). As the pin probe rotates and proceeds in the direction of the weld, the plasticized material is extruded to the back of the tool where it is forged and consolidated under hydrostatic pressure (Ref 7, 8). The intense plastic deformation in this process creates a fully recrystallized, equiaxed, and fine-grained microstructure in the weld nugget. This novel solid state joining process has been used to join or process aluminum alloys (Ref 9), mild steels (Ref 6, 8, 10), titanium alloys (Ref 11), oxide dispersion strengthened (ODS) alloys (Ref 12), metal matrix composites (Ref 13), dissimilar alloys (Ref 14), and nickel alloys (Ref 15, 16). Recently, FSW has also been used for microstructural modification, grain refinement, and inducing superplasticity (Ref 17-20).

As a solid state joining process that requires no filler material, FSW avoids the problems associated with the filler metal and the liquid state. Compared with conventional fusion welding processes, FSW offers improved mechanical properties, reduced distortion, increased fatigue life, and minimal residual stresses (Ref 21-24). Three essential FSW variables (rotational speed, travel speed, and plunge depth) determine the microstructure of a friction stir weld by controlling the heat input to the weld (Ref 6). A measure of energy input per unit weld length is the *Specific Weld Energy* (Ref 25) defined as

$$E = \frac{\omega\tau}{s}, \quad \mathrm{J\,mm^{-1}} \qquad \text{(Eq 1)}$$

where ω = pin tool angular velocity, radians s^{-1}, τ = pin tool torque, N m, s = tool travel velocity, mm s^{-1}.

Bharat K. Jasthi, William J. Arbegast, and **Stanley M. Howard**, Department of Materials and Metallurgical Engineering, Advanced Materials Processing Center, South Dakota School of Mines and Technology, 501 E. Saint Joseph St., Rapid City, SD 57701. Contact e-mail: jasthi@gmail.com.

Pin tool rotation velocity throughout this paper is reported as rev min^{-1}, which differs from ω (radians s^{-1}) by 2π/60. A thorough review of the FSW process and technology is available in the literature (Ref 26).

2. Experimental

High-temperature pin tools made of polycrystalline BN (PCBN) and W-25%Re (W-Re) were used to make bead-on-plate FSW welds on Invar plates (12.7 × 95.2 × 609.6 mm). Each weld was 76 mm long and made using an MTS-*i*stir-10® FSW system equipped with a Megastir® water-cooled, high-temperature pin tool (HTPT) adapter. This multiaxis machine is fitted with an AdAPT® (adjustable and adaptable pin tool) head (Fig. 1) that has the advantage of welding complex shapes and also can eliminate the exit hole by slowly retracting the pin probe at the end of the weld. All the welds were made using a controlled shoulder plunge depth of 0.0127 mm. Both tools had a 6.35 mm pin probe length and a concave shoulder and a frustum-shaped pin probe with three flats. The tool-to-workpiece angle was maintained at 3.5° for all the welds. Figure 2 shows the pin tools, clamping, and welding setup used for FSW of Invar plates. The pitch axis of the AdAPT® head was isolated using hard mechanical stops to minimize potential damage to the pin tools, especially the PCBN tool. The Megastir® HTPT adapter radio-frequency telemetry system was used to monitor the temperature of the friction stir welds at a location immediately above the pin tool shoulder. The tools and Invar were shielded with Ar gas during welding to prevent oxidation. Different combinations of rotational and translational speeds were employed in this investigation as summarized in Table 1.

The *X*-force (sliding) is the force in the direction of weld travel. The *Y*-force (separation) is transverse to the direction of travel and the *Z*-force (forge) is applied normal to the workpiece surface. These forces were measured at a sampling rate of 20.1 Hz using sensors embedded in the MTS-*i*stir-10® system.

After welding, the plates were sectioned perpendicular to the welding direction and prepared for metallographic examination using standard metallographic polishing procedures. The polished specimens were etched with a solution consisting of

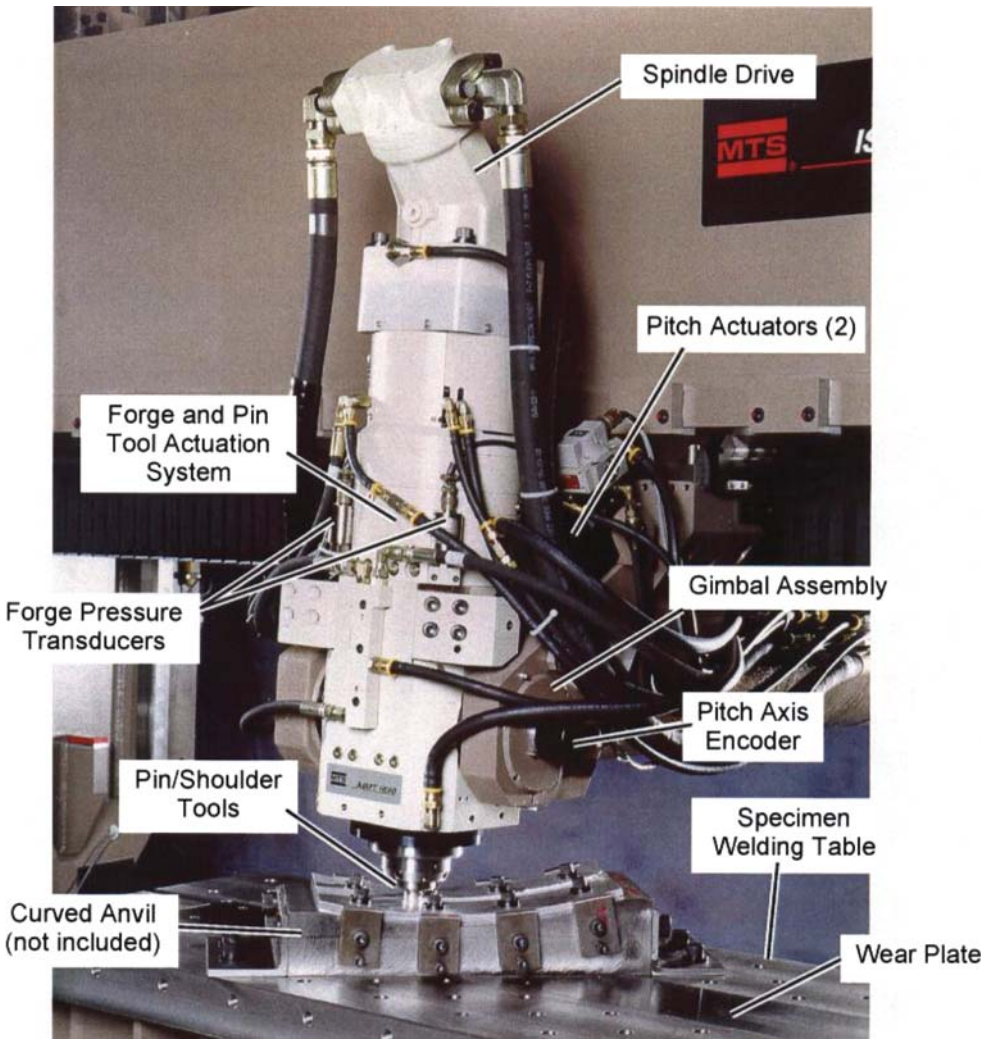

Fig. 1 Multiaxis AdAPT FSW head at Advanced Materials Processing Center of South Dakota School of Mines and Technology

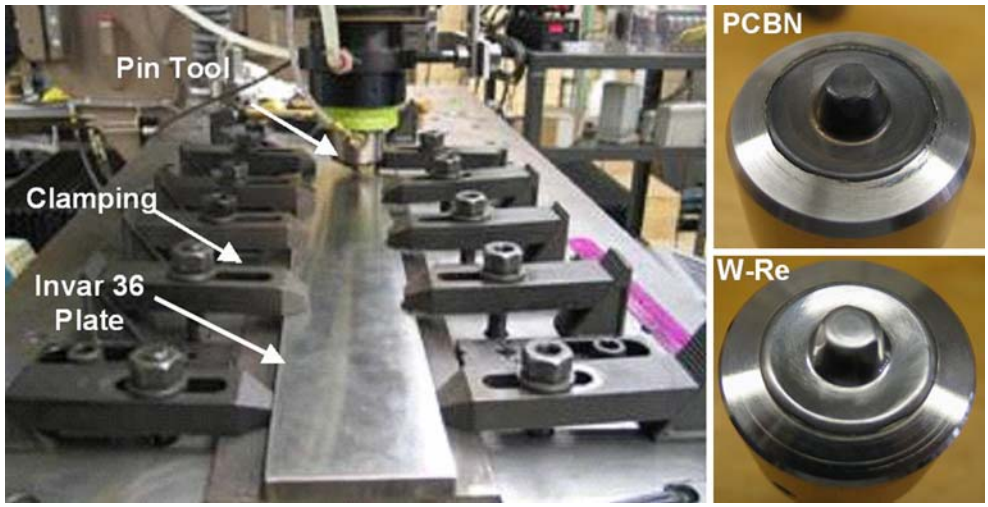

Fig. 2 Friction stir welding setup showing Invar plate, clamping, and pin tools

Table 1 Friction stir welding process parameters used for making welds

Pin tool	Travel speed, mm min^{-1}	Rotational speed, rev min^{-1}
PCBN	76, 102, 127	500
PCBN	76, 102, 127	600
W-Re	76, 102, 127	600

100 mL HCl, 2 g $CuCl_2$, 7 g $FeCl_3$, 5 mL HNO_3, 200 mL methanol, and 100 mL H_2O for 30 s. The specimens were examined using a metallurgical microscope. All samples in this investigation were cut while water-cooled.

Specimens ($8.0 \times 4.5 \times 4.0$ mm) for CTE measurements were cut from the parent metal and the FSW weld nuggets made at 600 rev min^{-1} rotational speed and 76, 102, and 127 mm min^{-1} travel speeds. The measurements were made using a thermomechanical analyzer (TMA) from 25 to 450 °C at the heating rate of 5 °C min^{-1} according to ASTM 831-03 (Ref 27). Measurements were obtained in the direction of the weld (longitudinal) and perpendicular to the weld direction (transverse).

Room temperature tensile test samples were cut transversely from welded FSW plates joined with both PCBN and W-Re pin tools using the optimal parameters of 600 rev min^{-1} and 127 mm min^{-1} as determined by a series of preliminary welds. The ultimate tensile strength (UTS), yield strength (YS), and percent elongation were recorded for each specimen. Specimens (12.7 mm thick) for the tensile testing for the welds made with W-Re pin tool were cut from the full thickness double-sided welds (welded top and bottom). The specimens made with PCBN tools (5.0 mm thick) were extracted from the partial penetration single-sided weld. The bottom part of the plate was machined to simulate a full penetration weld. Vickers microhardness measurements were made across the weld nugget at a distance of 3.0 mm from the top of the weld and at a horizontal spacing of 0.25 mm across the polished metallographic weld cross sections. The measurements were made at a load of 500 g and a loading time of 15 s in accordance with ASTM E92-82 (Ref 28).

X-ray radiography (160 kV, 5 mA, 60 s) was performed on the welds to identify possible defects and weld contamination from the pin tools. The source-to-film distance was kept at 711 mm. Invar and the pin tool materials have much different absorption characteristics, which facilitated finding weld contamination. A scanning electron microscope (SEM) energy dispersive X-ray (EDX) analysis was performed on the specimens in the unetched condition to verify the composition of presumed weld nugget contamination.

3. Results

Figure 3(a) shows the *X*- and *Z*-forces as function of pin tool travel speed. The use of pitch isolator system for minimizing the potential damage to the pin tools made *Y*-forces suspect. Therefore, they are not reported. Peak temperatures measured during welding as a function of travel speed are shown in Fig. 3(b). The variation of specific weld energy with travel speed is shown in Fig. 3(c). Figure 4 shows the microstructures of the Invar before and after welding with each pin tool. CTE measurement results for material welded with each pin tool material at 600 rev min^{-1} are shown in Fig. 5.

Figure 6 shows close-up photographs of the pin tools before and after welding. Radiographic results for the welds made with the PCBN and the W-Re pin tools are shown in Fig. 7. Figure 8 is a high magnification micrograph and EDX spectrum for the remnants left in the weld by the W-Re pin tool evident in Fig. 7(d). Hardness profiles across the weld nugget are shown in Fig. 9. Results of the tensile measurements are tabulated in Table 2. The reported tensile results are the average of two specimens for the welds and the parent material.

4. Discussion

Four topics are of great importance to any consideration of FSW to join Invar: (1) weld process response of the material (effect of FSW parameters on weld quality), (2) microstructural

and CTE properties of the optimally welded material, (3) possible pin tool remnants in the weld as determined by radiographic analysis, and (4) mechanical properties of the weld.

4.1 Weld Process Responses

Comparisons of *X*- and *Z*-forces as a function of travel speed for welds made with both pin tools at 600 rev min^{-1} shown in Fig. 3(a) are the average values from the steady state section of the weld. The W-Re pin tool forces were significantly lower than those for the PCBN pin tool. The *X*-force is an important variable since this bending stress causes pin tool breakage. The *X*-force increased with travel speed. Increasing the *Z*-force also increases the probability of tool breakage, especially for PCBN tools. Tool life is extended by lowering these forces. The lower forces observed for W-Re pin tool is believed to be the consequence of its lower thermal conductivity, which translates to lower heat loss through the tool and higher Invar temperatures.

The lower temperatures reported for the PCBN pin tool compared to the W-Re pin tool are the result of relative thermal conductivity differences (PCBN 100-250, W-Re 55-65 W m^{-1} K^{-1}) in the pin tools. Since the PCBN pin tool has the higher thermal conductivity, it conducts the same heat with a smaller temperature gradient than does the W-Re pin tool.

Since the pin tool-Invar interface is some distance (~10 mm) from the thermocouple used to measure the temperatures reported in Fig. 3(b), the actual weld temperatures are higher by perhaps few hundred Celsius degrees. The trend of decreasing measured temperatures corresponds well with the decreasing specific weld energy with increasing weld speed shown in Fig. 3(c) and as expected from Eq 1.

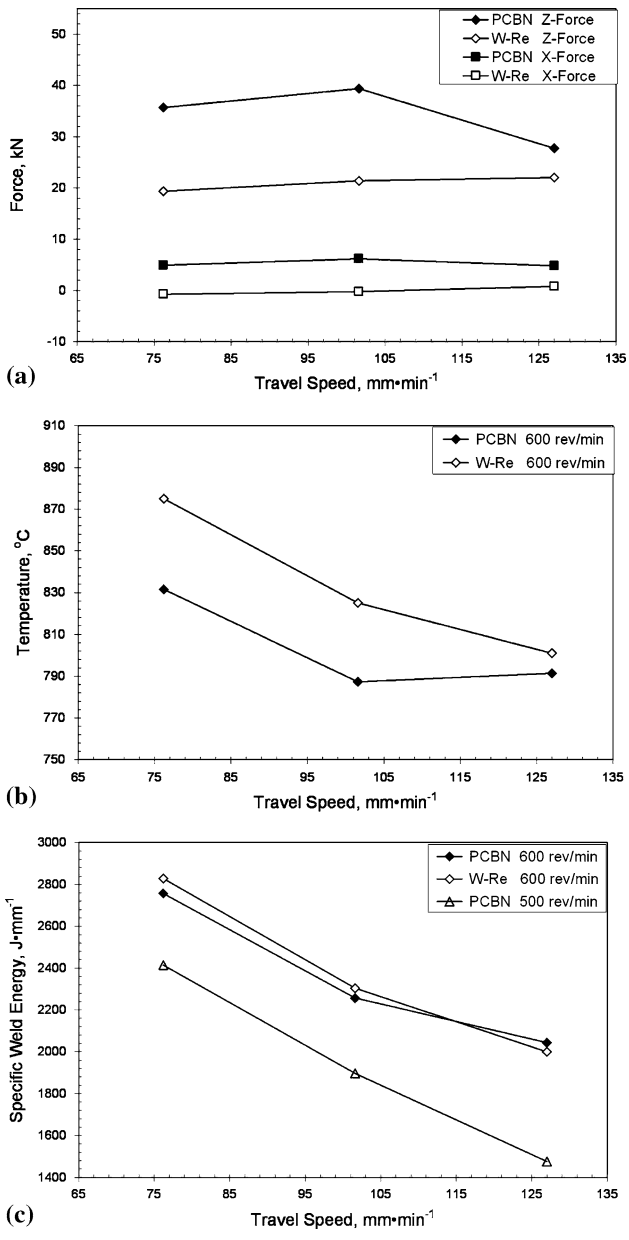

Fig. 3 Comparison of weld process responses as a function of travel speed for welds made with PCBN and W-Re pin tools showing: (a) *X*-force and *Z*-force; (b) peak temperatures; and (c) specific weld energies

4.2 Microstructural Characterization and CTE Studies

The parent metal has an austenite grain structure with a high density of twins shown in Fig. 4(a). The micrographs of the weld nuggets that were processed with PCBN and W-Re pin tools and at 600 rev min^{-1} and 127 mm min^{-1} are shown in Fig. 4(b) and (c). The grains in the weld nugget regions are relatively coarser and had a lower density of twins than the parent material shown in Fig. 4(a). The microstructure throughout the weld nugget region was not uniform and a large variation in grain size was observed. Very fine grains were observed in the crown region of the welds and relatively coarser grains were observed in the weld nugget region. A slight increase in grain size was observed in the thermo-mechanical-affected zone, which lies between the weld nugget and parent material. The heterogeneous nature of the deformation in the processed region explains the observed microstructural variations.

The fine, equiaxed, and recrystallized grains in the weld nugget shown in Fig. 4(d) are observed on the advancing side. This is the side of the weld nugget where the direction of tool travel is same as the direction of pin tool rotation. These recrystallized grains were only observed for the welds made with the PCBN tools, which suggests a temperature-related effect since thermal conductivity is the salient difference in the pin tools used. The same fine-grain structure in the nugget region of aluminum alloys is attributed to dynamic recrystallization (Ref 29-31). Proposed mechanisms for this effect include discontinuous, continuous, and geometric dynamic recrystallization (Ref 26, 32).

Each CTE point in Fig. 5, which is the average of three tests in each orientation, shows there is no significant difference in CTE between the weld nugget and the parent material in both the longitudinal and transverse directions. Also the pin tool material had no effect on the measured CTE. Likewise, pin tool travel speed has no significant effect on the coefficient of thermal expansion regardless of the pin tool material used.

4.3 X-ray Radiographic Analysis

The SEM backscattered image of weld nugget showing the W-Re pin tool remnants shown in Fig. 8(a) was confirmed by

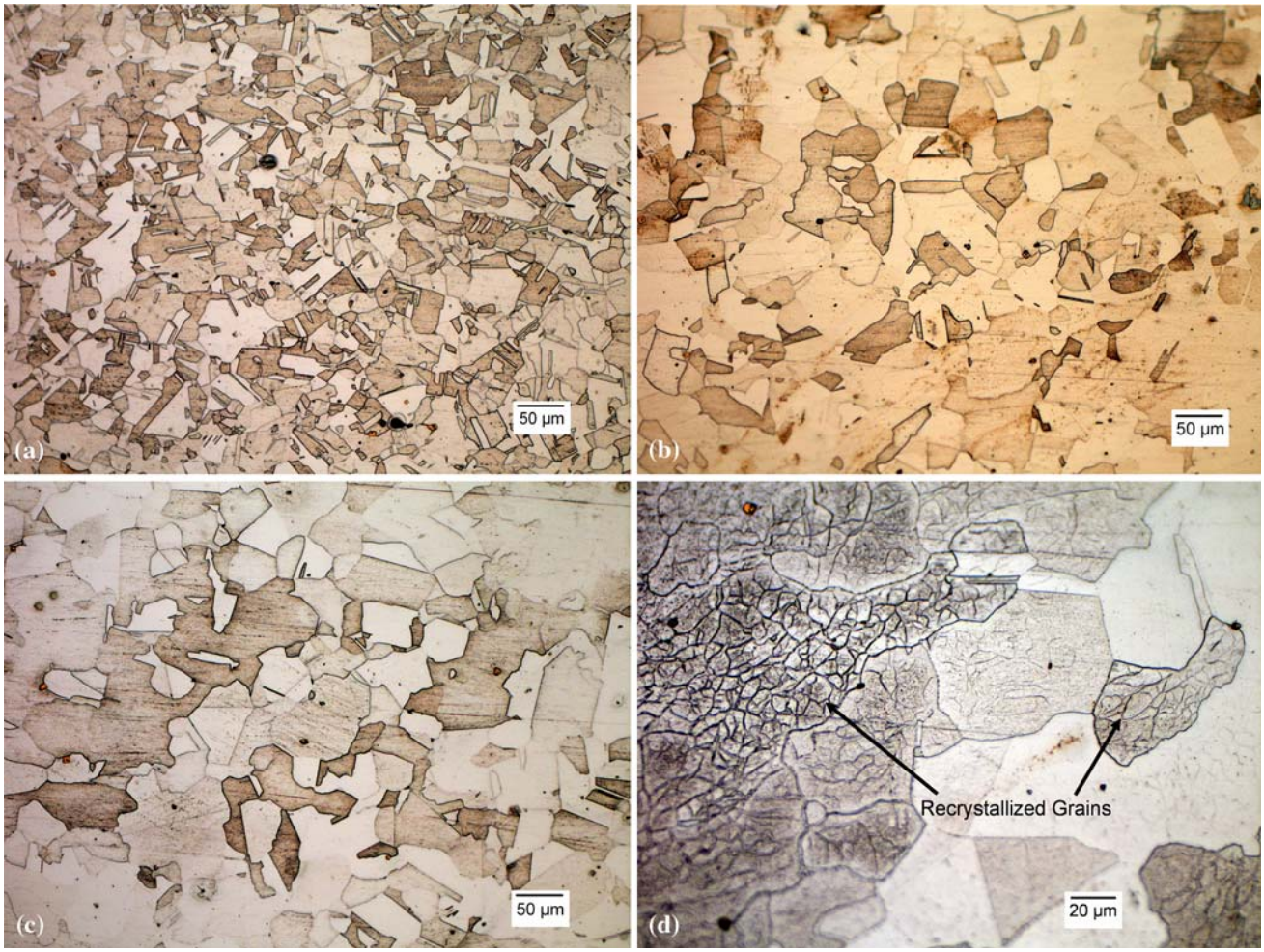

Fig. 4 Micrographs of Invar showing: (a) parent material; (b) nugget region processed with PCBN pin tool; (c) nugget region processed with W-Re pin tool; and (d) recrystallized grains in the weld nugget that is processed with PCBN pin tool

SEM EDX analysis as shown in Fig. 8(b). The severe wear and degradation of the W-Re pin tool for even the short welds distances were not unexpected since the W-Re alloy is not designed for wear resistance. Conversely, the inconsequential PCBN pin tool wear is to be expected since PCBN is a much harder material known for its wear properties.

No wear debris was identified in the welds made with the PCBN pin tool. This is not surprising since the PCBN pin tools showed no significant wear. On the other hand, the significant wear of the W-Re pin tool corresponds to the substantial debris appearing in Fig. 7(d). The debris was greatest during the initial weld plunge during which time the pin tool undergoes the greatest duress. Little debris was observed during the steady state portion of the weld. Debris was concentrated on the retreating side of the weld. Possible strategies for decreasing the wear of the W-Re tool includes preheating the Invar plate before welding, lowering the rotational speeds, and providing sufficient inert cover gas to prevent oxidation.

X-ray radiography not only aided in identification of pin tool remnants, but also identified a wormhole defect formed during the welding process at 500 rev min^{-1} made at 127 mm min^{-1} travel speeds using the PCBN tool as shown in Fig. 7(b). The defect did not appear when the weld speed was decreased to 76 mm min^{-1}, which is a relatively hotter weld. The dark lines perpendicular to the welding direction indicate cuts made of the welds before the X-ray radiographic analysis.

4.4 Mechanical Properties Evaluation

The hardness profiles show that neither the pin tool nor the pin tool travel speeds used for welding had an effect on hardness across the nugget or heat-affected zone. This is not unexpected because the alloy is not heat treatable. Similar response is observed for nonheat-treatable aluminum alloys (Ref 26). Conversely, many heat-treatable aluminum alloys exhibit a softened region in the weld nugget likely caused by the dissolution and coarsening of the strengthening precipitates during friction stir welding (Ref 33-36).

The transverse tensile test results from Table 2 show that the ultimate strengths for the welds (453 MPa for W-Re and 461 MPa for PCBN) were essentially the same as the parent material (461 MPa). All the welded specimens failed within the nugget region. The elongation for the parent material was 52% while elongations of 30 and 37% were achieved for the welds made with the W-Re and the PCBN pin tools. Welds made with W-Re pin tools showed pin tool material contamination in all of the welds. Examination of the W-Re fractured tensile specimens suggested a very small unwelded region in the center

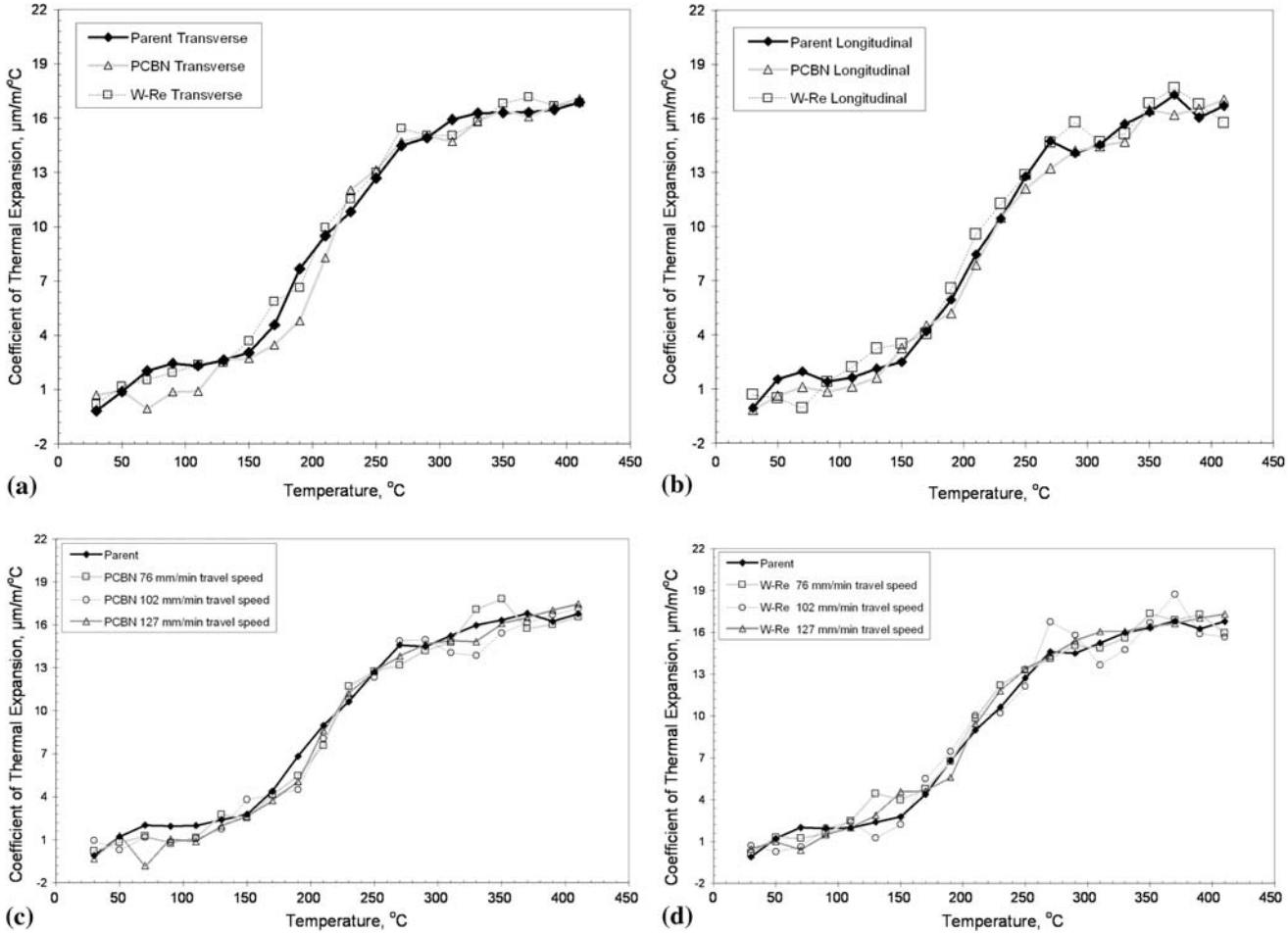

Fig. 5 Comparison of CTE between Invar parent material and friction stir welds that were processed at 600 rev min^{-1} rotational speed: (a) in transverse direction; (b) in longitudinal direction; (c) for welds made with PCBN pin tool; and (d) for welds made with W-Re pin tool

Fig. 6 Appearance of PCBN and W-Re pin tools before and after friction stir welding of Invar

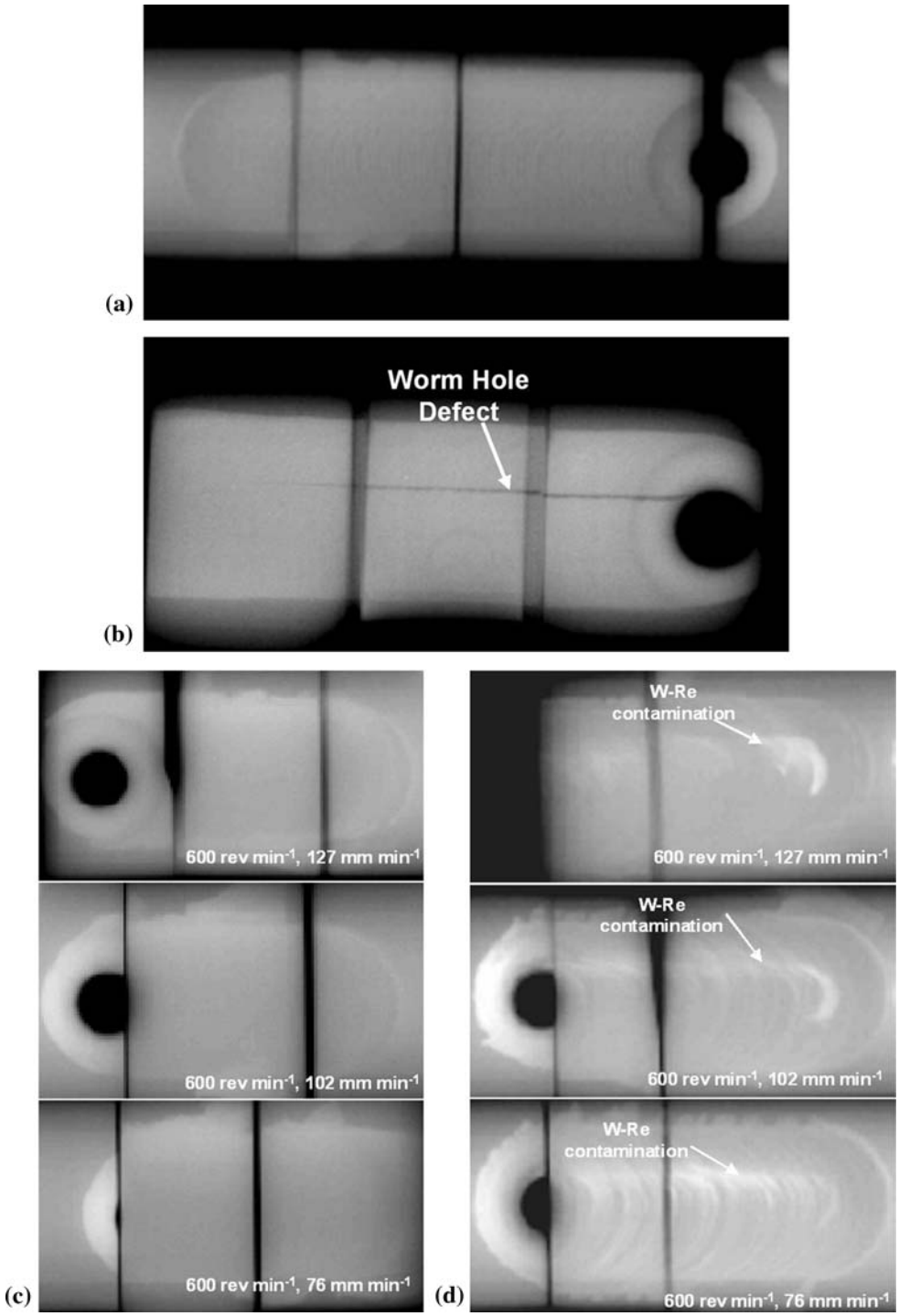

Fig. 7 X-ray radiographic analysis of the friction stir welds showing: (a) defect-free weld when processed at 76 mm min^{-1} and 500 rev min^{-1} with PCBN pin tool; (b) wormhole defect when processed at 127 mm min^{-1} and 500 rev min^{-1} with PCBN pin tool; (c) good welds with no contamination when processed with PCBN tool; and (d) W-Re contamination in welds when processed with W-Re pin tool

caused by a minor overlap mismatch of the double-sided weld. This and the contamination are possible reasons for the lower elongation of the W-Re welds.

Gottlieb and Shira reported ultimate strengths of 407 MPa and elongations in the range of 8-14% for gas tungsten arc welded (GTAW) Invar when similar-to-Invar filler metal was used (Ref 3). The FSW-produced joints exhibit higher strengths and elongations than the GTAW process. This is attributed to the solid state nature of FSW process, which produces a wrought microstructure with narrow heat-affected zones rather than a cast microstructure as produced by fusion welding. Fusion welding creates a joint by locally melting the material with subsequent solidification. The melting is subject to cracking, porosity, segregation, and contamination. These may result in degraded joint properties. Solid state joining nature of the FSW avoids these undesirable characteristics.

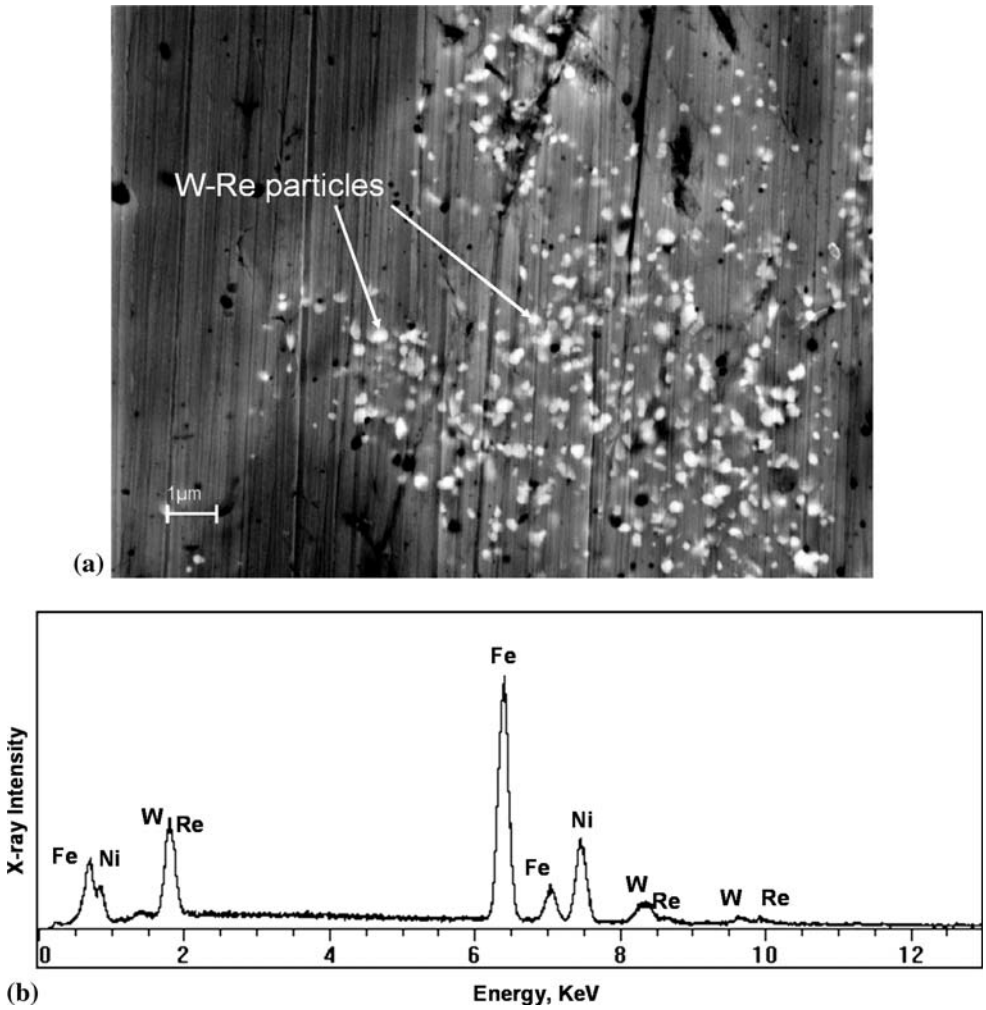

Fig. 8 SEM analysis of the Invar weld that is processed with W-Re pin tool showing: (a) backscattered image of the weld nugget region showing pin tool remnants and (b) EDX analysis showing Fe, Ni, W, and Re peaks

Even though X-ray radiographic studies confirmed the presence of W-Re pin tool remnants in the welds, the mechanical properties (except elongation) and the CTE of the welded material were essentially the same as for the welds made with the PCBN pin tool and the parent material. This indicates that the remnant concentration in the specimens extracted from the central region of the weld was below a minimal threshold consequential to the reported mechanical and thermal properties.

PCBN is a super abrasive with excellent wear resistance and chemical stability at elevated temperatures. They are manufactured at ultrahigh temperature and pressures, which makes them expensive. These tools have very low fracture toughness and hence require great care during welding to avoid breakage. Slow penetration and retraction and very low eccentric spindle movement must be observed to minimize tool fracture.

PCBN tools produce clean welds with no contamination in Invar and can be used to produce contamination-free welds. W-Re pin tools are relatively cheaper and have a better fracture toughness but have inferior wear resistance compared to PCBN tools. W-Re pin tools have been able to produce good quality (defect free) welds in Invar but their poor wear characteristics makes problematic their use in a continuous production environment. However, they can be used for periodic welding or repair applications if W-Re contamination in the weld is not an issue.

5. Conclusions

Friction stir welding of Invar eliminates solidification cracking, porosity, reheating cracking, and other severe problems associated with the fusion welding; produces joints with good mechanical properties; and results in an isotropic CTE that matches the parent material. Excellent welds were produced with both PCBN and W-Re pin tools at a rotational speed of 600 rev min^{-1} and travel speeds of 76, 102, and 127 mm min^{-1}. A wormhole defect was observed in the weld produced with the PCBN pin tools at a rotational speed of 500 rev min^{-1} and 127 mm min^{-1} travel speed.

The coefficients of thermal expansion, tensile strength, and microhardness of the welds were essentially unchanged from the parent material. The welded CTE was unaffected by pin tool material or weld parameters. The measured elongation was 52% for the parent material and 30 and 37% for the welds made

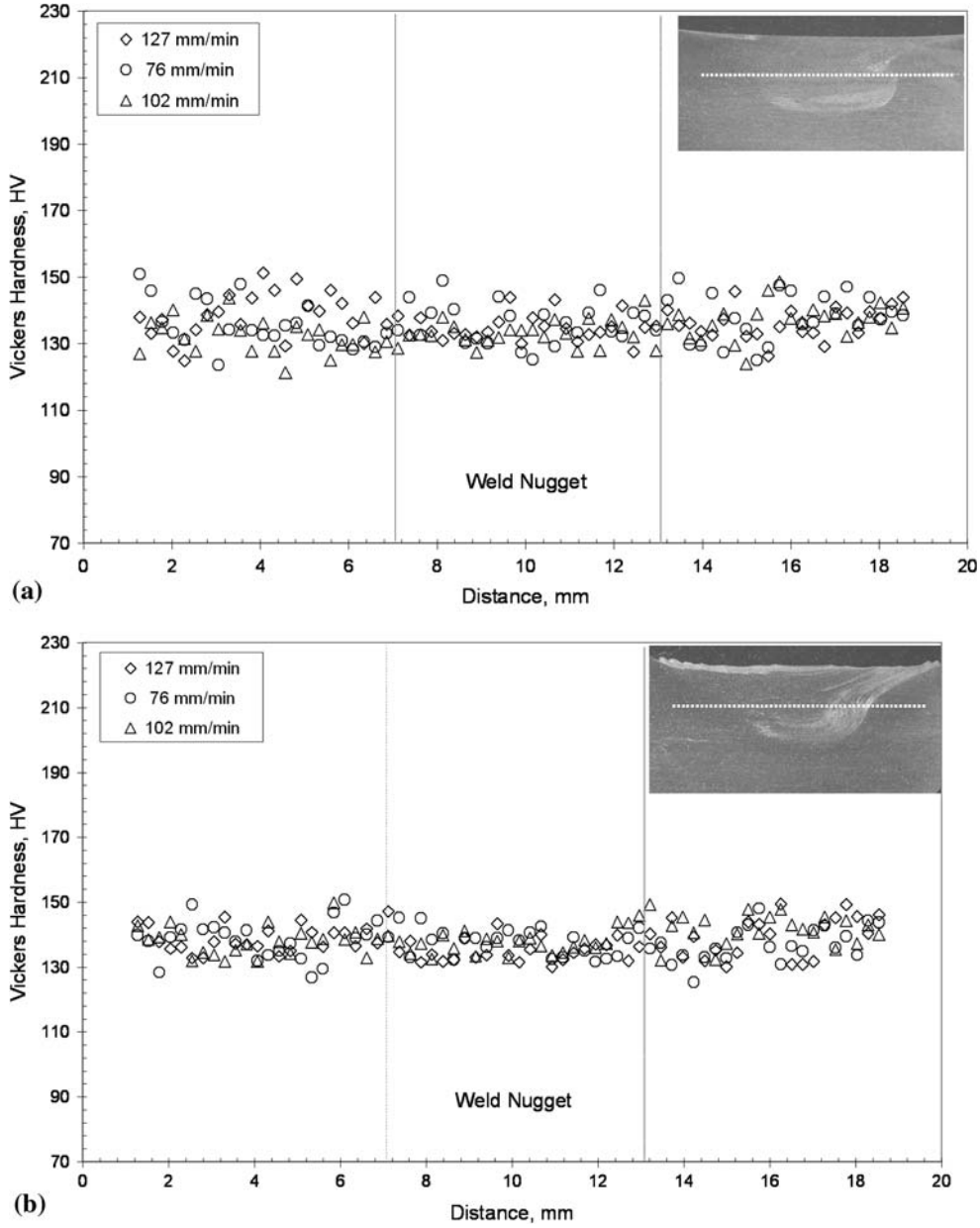

Fig. 9 Vickers hardness profiles across the weld nugget in Invar for welds made at 600 rev min^{-1} rotational speed and different travel speeds for welds made with: (a) PCBN pin tool and (b) W-Re pin tool

Table 2 Transverse tensile properties of Invar's parent metal and friction stir welds

	Parent metal	Welds made with W-Re pin tool	Welds made with PCBN pin tool
Ultimate strength, MPa	461 ± 7	453 ± 4	461 ± 0
Yield strength, MPa	292 ± 15	255 ± 0	296 ± 17
Elongation, %	52 ± 1	30 ± 1	37 ± 5

with W-Re and PCBN pin tools. The PCBN pin tool produced remnant-free welds with insignificant tool wear, but the W-Re pin tool showed significant wear and left tool remnants in the weld.

Acknowledgments

This research was sponsored by the Army Research Laboratory (ARL) and performed under Cooperative Agreement Number DAAD19-02-2-0011. The authors gratefully acknowledge SGT. Troy Hannon and staff, Ellsworth Air Force Base, Ellsworth, SD, for making available the X-ray radiography facility. The authors also acknowledge Dr. William Cross, South Dakota School of Mines and Technology for his support regarding the TMA analysis.

References

1. W.H. Otte, D.B. O'Donnell, S.D. Kiser, and C.W. Cox, Welding Low Thermal Expansion Alloys for Aircraft Composite Tooling, *Weld. J.*, 1996, **75**(7), p 51–55

2. C.E. Witherell, Welding Nickel-Iron Alloys of the Invar Type, *Weld. J.*, 1964, **43**(4), p 161-s–169-s
3. T. Gottlieb and C.S. Shira, Fabrication of Iron-Nickel Alloys for Cryogenic Piping Service, *Weld. J.*, 1965, **44**(3), p 116-s–123-s
4. T. Ogawa, Weldability of Invar and Its Large-Diameter Pipe, *Weld. J.*, 1986, **65**(8), p 213-s–226-s
5. W.M. Thomas, E.D. Nicholas, J.C. Needham, M.G. Murch, P. Templesmith, and C.J. Dawes, Friction Stir Butt Welding, International Patent App. No. PCT/GB92/02203 and GB Patent App. No. 9125978.8, December 1991, U.S. Patent No. 5,460,317, October 1995
6. W.M. Thomas, Friction Stir Welding of Ferrous Materials: A Feasibility Study, *Proceedings of the 1st International Symposium on Friction Stir Welding*, June 14-16, 1999 (Thousand Oaks, CA, USA), TWI, 1999, cd-rom
7. W.J. Arbegast, Modeling Friction Stir Joining as a Metal Working Process, *Hot Deformation of Aluminum Alloys-III*, Z. Jin, A. Beaudoin, T.A. Bieler, and B. Radhakrishnan, Eds., March 2-6, 2003 (San Diego, USA), The Minerals, Metals & Materials Society, 2003, p 313–327
8. T.J. Lienert and J.E. Gould, Friction Stir Welding of Mild Steel, *Proceedings of the 1st International Symposium on Friction Stir Welding*, June 14-16, 1999 (Thousand Oaks, CA, USA), TWI, 1999, cd-rom
9. W.J. Arbegast and P.J. Hartley, Friction Stir Weld Technology Development at Lockheed Martin Michoud Space Systems—An Overview, *Proceedings of the 5th International Conference on Trends in Welding Research*, June 1-5 (Pine Mountain, GA, USA), 1998, p 541–546
10. B.M. Tweedy, W.J. Arbegast, and C.D. Allen, Friction Stir Welding of Ferrous Alloys Using Induction Preheating, *Friction Stir Welding and Processing-III*, K.V. Jata, M.W. Mahoney, R.S. Mishra, and T.J. Lienert, Eds., February 13-17, 2005 (San Francisco, USA), The Minerals, Metals and Materials Society, 2005, p 97–104
11. R.L. Goetz and K.V. Jata, Modeling Friction Stir Welding of Titanium and Aluminum Alloys, *Friction Stir Welding and Processing*, K.V. Jata, M.W. Mahoney, R.S. Mishra, S.L. Semiatin, and D.P. Field, Eds., November 4-8, 2001 (Indianapolis, USA), The Minerals, Metals and Materials Society, 2001, p 35–42
12. B.K. Jasthi, S.M. Howard, W.J. Arbegast, G.J. Grant, S. Koduri, and D.R. Herling, Friction Stir Welding of MA 957 Oxide Dispersion Strengthened Ferritic Steel, *Friction Stir Welding and Processing-III*, K.V. Jata, M.W. Mahoney, R.S. Mishra, and T.J. Lienert, Eds., February 13-17, 2005 (San Francisco, USA), The Minerals, Metals and Materials Society, 2005, p 75–79
13. R.A. Prado, L.E. Murr, D.J. Shindo, and J.C. McClure, Friction Stir Welding: A Study of Tool Wear Variation in Aluminum Alloy 6061 + 20% Al_2O_3, *Friction Stir Welding and Processing*, K.V. Jata, M.W. Mahoney, R.S. Mishra, S.L. Semiatin, and D.P. Field, Eds., November 4-8, 2001 (Indianapolis, USA), The Minerals, Metals and Materials Society, 2001, p 105–116
14. J. Ouyang, E. Yarrapareddy, and R. Kovacevic, Microstructural Evolution in the Friction Stir Welded 6061 Aluminum Alloy (T6-temper condition) to Copper, *J. Mater. Process. Technol.*, 2006, **172**(1), p 110–122
15. C.D. Sorensen, B. Nelson, and S. Sanderson, Properties and Structure of Friction Stir Welded Alloy 718, *Friction Stir Welding and Processing-IV*, R.S. Mishra, M.W. Mahoney, T.J. Lienert, and K.V. Jata, Eds., February 25-March 1, 2007 (Orlando, USA), The Minerals, Metals and Materials Society, 2007, p 285–293
16. B.K. Jasthi, S.M. Howard, C.D. Allen, and W.J. Arbegast, Effects of Friction Stir Welding on the Coefficient of Thermal Expansion of Invar 36, *Friction Stir Welding and Processing-IV*, R.S. Mishra, M.W. Mahoney, T.J. Lienert, and K.V. Jata, Eds., February 25-March 1, 2007 (Orlando, USA), The Minerals, Metals and Materials Society, 2007, p 303–309
17. R.S. Mishra, M.W. Mahoney, S.X. McFadden, N.A. Marra, and A.K. Mukarjee, High Strain Rate Superplasticity in a Friction Stir Processed 7075 Al Alloy, *Scripta Mater.*, 2000, **42**(2), p 163–168
18. Z.Y. Ma, R.S. Mishra, and M.W. Mahoney, Superplastic Deformation Behavior of Friction Stir Processed 7075Al Alloy, *Acta Mater.*, 2002, **50**(17), p 4419–4430
19. Z.Y. Ma and R.S. Mishra, Cavitation in Superplastic 7075Al Alloys Prepared via Friction Stir Processing, *Acta Mater.*, 2003, **51**(12), p 3551–3569
20. I. Charit and R.S. Mishra, High Strain Rate Superplasticity in a Commercial 2024 Al alloy via Friction Stir Processing, *Mat. Sci. Eng. A*, 2003, **359**(1–2), p 290–296
21. W.J. Arbegast, Friction Stir Welding after a Decade of Development, *Weld. J.*, 2006, **85**(3), p 28–35
22. W.J. Arbegast, K.S. Baker, and P.J. Hartley, Fracture Toughness Evaluations of 2195 Al-Cu-Li Autogenous and Hybrid Friction Stir Welds, *Proceedings of the 5th International Conference on Trends in Welding Research*, June 1-5 (Pine Mountain, GA, USA), 1998, p 558–562
23. B.J. Dracup and W.J. Arbegast, Friction Stir Welding as a Rivet Replacement Technology, U.S. Patent App. No. 6,986,452, B2 17 Jan 2006
24. Z.X. Li, W.J. Arbegast, and P.J. Hartley, Microstructure Characterization and Stress Corrosion Evaluation of Friction Stir Welded AL 2195 and Al 2219 Alloys, *Proceedings of the 5th International Conference on Trends in Welding Research*, June 1-5 (Pine Mountain, GA, USA), 1998, p 568–573
25. A.P. Reynolds and W. Tang, Alloy, Tool Geometry, and Process Parameter Effects on Friction Stir Weld Energies and Resultant FSW Joint Properties, *Friction Stir Welding and Processing*, K.V. Jata, M.W. Mahoney, R.S. Mishra, S.L. Semiatin, and D.P. Field, Eds., November 04-08, 2001 (Indianapolis, USA), The Minerals, Metals and Materials Society, 2001, p 15–23
26. R.S. Mishra and Z.Y. Ma, Friction Stir Welding and Processing, *Mater. Sci. Eng. R.*, 2005, **50**(1–2), p 1–78
27. Standard Test Method for Linear Thermal Expansion of Solid Materials by Thermomechanical Analysis, E831-06, *Annual Book of ASTM Standards, Part 14.02*, ASTM, 2000, p 348–352
28. Standard Test Method for Vickers Hardness of Metallic Materials, E92-82, *Annual Book of ASTM Standards, Part 03.01*, ASTM, 1996, p 206–214
29. J.Q. Su, T.W. Nelson, and C.J. Sterling, Microstructure Evolution During FSW/FSP of High Strength Aluminum Alloys, *Mat. Sci. Eng. A*, 2005, **405**(1–2), p 277–286
30. K.V. Jata and S.L. Semiatin, Continious Dynamic Recrystallization During Friction Stir Welding of High Strength Aluminum Alloys, *Scripta Mater.*, 2000, **43**(8), p 743–749
31. Y.S. Sato, M. Urata, and H. Kokawa, Parameters Controlling Microstructure and Hardness During Friction-stir Welding of Precipitation-Hardenable Aluminum Alloy 6063, *Metall. Mater. Trans. A*, 2002, **33**(3), p 625–635
32. R.D. Doherty, D.A. Hughes, F.J. Humphreys, J.J. Jonas, D.J. Jensen, M.E. Kassner, W.E. King, T.R. McNelley, H.J. McQueen, and A.D. Rollett, Current Issues in Recrystallization: A Review, *Mater. Sci. Eng. A*, 1997, **238**(2), p 219–274
33. S. Benavides, Y. Li, L.E. Murr, D. Brown, and J.C. McClure, Low-Temperature Friction-stir Welding of 2024 Aluminum, *Scripta Mater.*, 1999, **41**(8), p 809–815
34. Y. Li, L.E. Murr, D. Brown, and J.C. McClure, Flow Visualization and Residual Microstructures Associated with the Friction-stir Welding of 2024 Aluminum to 6061 Aluminum, *Mater. Sci. Eng. A.*, 1999, **271**(1–2), p 213–223
35. Y.S. Sato, H. Kokawa, M. Enomoto, and S. Jogan, Microstructural Evolution of 6063 Aluminum During Friction-stir welding, *Metall. Mater. Trans. A*, 1999, **30**(9), p 2429–2437
36. Y.S. Sato, H. Kokawa, K. Ikeda, M. Enomoto, T. Hashimoto, and S. Jogan, Microtexture in the Friction-stir Weld of an Aluminum Alloy, *Metall. Mater. Trans. A*, 2001, **32**(4), p 941–948